Nuclear Instruments and Methods in Physics Research A 703 (2013) 183–189

Contents lists available at SciVerse ScienceDirect

Nuclear Instruments and Methods in Physics Research A

journal homepage: www.elsevier.com/locate/nima

Development of an ultrahigh-resolution Si-PM-based dual-head GAGG coincidence imaging system ☆

Seiichi Yamamoto [a,*], Hiroshi Watabe [b], Yasukazu Kanai [b], Katsuhiko Kato [a], Jun Hatazawa [b,c]

[a] Department of Radiological and Medical Laboratory Sciences, Nagoya University Graduate School of Medicine, Japan
[b] Department of Molecular Imaging in Medicine, Osaka University Graduate School of Medicine, Osaka, Japan
[c] Department of Nuclear Medicine and Tracer Kinetics, Osaka University Graduate School of Medicine, Osaka, Japan

ARTICLE INFO

Article history:
Received 17 August 2012
Received in revised form
18 November 2012
Accepted 20 November 2012
Available online 29 November 2012

Keywords:
Si-PM
Coincidence
Imaging
Ultra high resolution
GAGG

ABSTRACT

A silicon photomultiplier (Si-PM) is a promising photodetector for high resolution PET systems due to its small channel size and high gain. Using Si-PMs, it will be possible to develop a high resolution imaging systems. For this purpose, we developed a small field-of-view (FOV) ultrahigh-resolution Si-PM-based dual-head coincidence imaging system for small animals and plant research. A new scintillator, Ce doped $Gd_3Al_{12}Ga_3O_{12}$ (GAGG), was selected because of its high light output and its emission wavelength matched with the Si-PM arrays and contained no radioactivity. Each coincidence imaging block detector consists of $0.5 \times 0.5 \times 5$ mm^3 GAGG pixels combined with a 0.1-mm thick reflector to form a 20×17 matrix that was optically coupled to a Si-PM array (Hamamatsu MPPC S11064-050P) with a 1.5-mm thick light guide. The GAGG block size was 12.0×10.2 mm^2. Two GAGG block detectors were positioned face to face and set on a flexible arm based detector stand. All 0.5 mm GAGG pixels in the block detectors were clearly resolved in the 2-dimensional position histogram. The energy resolution was 14.4% FWHM for the Cs-137 gamma ray. The spatial resolution was 0.7 mm FWHM measured using a 0.25 mm diameter Na-22 point source. Small animal and plant images were successfully obtained. We conclude that our developed ultrahigh-resolution Si-PM-based dual-head coincidence imaging system is promising for small animal and plant imaging research.

1. Introduction

A high resolution PET system is needed for high resolution imaging for small animal PET studies. Although block detectors using smaller scintillators must be developed to realize a high resolution PET system, small scintillators are difficult to resolve using the Anger principle because of their relatively low light output and the relatively large channel size of the photodetectors because the resolving power of the Anger principle is roughly determined by the light output of the scintillators and the photodetector sizes [1].

A silicon photomultiplier (Si-PM) is a newly developed silicon-based photodetector that is also called a Geiger mode avalanche photodiode (G-APD) [2,3]. This photon counting device consists of multiple APD pixels operating in a Geiger mode. Some block detector designs [4–7] and small animal PET systems were already reported [8,9]. We recently developed a Si-PM-based depth-of-interaction (DOI) PET system using a phoswich structure for small animals that employed 16 detector blocks consisting of 4×4 Si-PM arrays and two types of Ce doped $Lu_{(1-x)}Gd_xSi0_5$ (LGSO) crystals with different decay times [8]. The block detector of the Si-PM-based PET system employed Hamamatsu 4×4 Si-PM arrays that were optically coupled with an 11×9 LGSO block of 1.1×1.2 mm^2 LGSO pixels. The position histogram for the 511 keV gamma ray had enough margins to use a much smaller scintillator, suggesting the possibility of developing an ultrahigh-resolution PET system with less than 1-mm scintillators. To clarify this possibility, we developed a 15×15 array LGSO block whose pixel size was $0.7 \times 0.7 \times 6$ mm^3 and combined it with a Si-PM array. We successfully resolved all LGSO pixels of the block detector [10]. We also developed an ultrahigh-resolution Si-PM-based compact gamma camera system for small animals that used $0.6 \times 0.6 \times 6$ mm^3 Ce doped Y_2SiO_5 (YSO) pixels to form a 17×17 matrix that was optically coupled to a Si-PM array [11]. Higher light output is desired to resolve smaller scintillators.

Ce doped $Gd_3Al_{12}Ga_3O_{12}$ (GAGG) is a newly developed scintillator that has large light output and longer light wavelength (500 nm) [12]. The longer wavelength of the scintillation light produces higher signals when it is combined with Si-PM since the

* Correspondence to: Department of Radiological and Medical Laboratory Sciences, Nagoya University Graduate School of Medicine, 1-1-20 Daiko-Minami, Higashi-ku 461-8673, Japan. Tel./fax: +81 52 719 1559.
E-mail address: s-yama@met.nagoya-u.ac.jp (S. Yamamoto).

☆ An ultrahigh-resolution Si-PM-based dual-head GAGG coincidence imaging system.

0168-9002/$ - see front matter © 2012 Elsevier B.V. All rights reserved.
http://dx.doi.org/10.1016/j.nima.2012.11.098

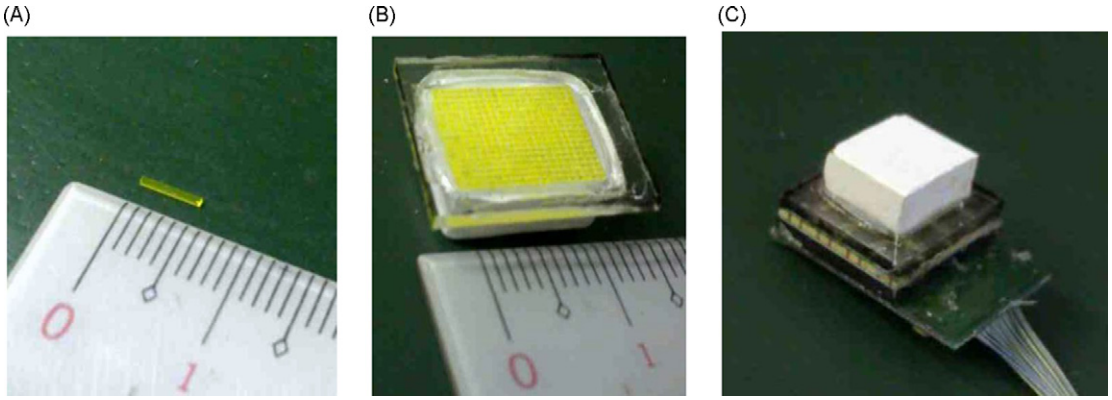

Fig. 1. $0.5 \times 0.5 \times 5$ mm^3 GAGG pixel (A), 20×17 GAGG block with 1.5-mm light guide (B) and, Si-PM based GAGG block detector (C).

Table 1
Comparison of property of scintillators.

Scintillator	Ce:GAGG	LYSO:Ce	BGO	CsI:Tl
Density (g/cm^3)	6.63	7.1	7.1	4.5
Light yield (ph/Mev)	46,000	30,000	8000	60,000
Decay time (ns)	90	40	300	1000
Peak emission (nm)	520	420	480	545
Energy resolution (%@662 keV)	4.9	9	12	5%

Si-PM's quantum efficiency is higher for the light with longer wavelength. Block detectors with higher resolution may be realized by combining the GAGG arrays with Si-PM arrays. Consequently, we developed an ultrahigh-resolution block detector using $0.5 \times 0.5 \times 5$ mm^3 GAGG pixels coupled with a Si-PM array and measured the performance. We also developed a dual-head coincidence imaging system using the block detectors, measured its performance, and demonstrated its usefulness in molecular imaging research. Although some dual-head coincidence imaging systems were developed for small animals and plants [13–15], most of those were used BGO, relatively low light output scintillators, and the spatial resolution was limited around 1.5–2 mm. In this paper, we show the system with less than 1 mm resolution by the use of GAGG scintillators.

2. Materials and methods

2.1. Si-PM-based GAGG block detector

Fig. 1(A) shows a single GAGG pixel used for the GAGG block. The GAGG pixel size was $0.5 \times 0.5 \times 5$ mm^3, and all the surfaces were mechanically polished (Furukawa Machine and Metal Co., Tokyo). The major properties of the GAGG are density of 6.6 g/cm^3, decay time of ~90 ns, light yield of ~46,000 photons/ MeV [12]. We listed the properties of scintillators in Table 1 for comparison [12].

The GAGG pixels were combined to form a 20×17 block with 0.1-mm thick $BaSO_4$ reflectors between them [16]. The outer size of the GAGG block was 12.0×10.2 mm^2. It was optically coupled to a 1.5-mm thick Acrylite (No. 000, Mitsubishi Rayon, Tokyo) light guide using a transparent silicone rubber (Shin-etsu Silicone, KE-420, Tokyo) (Fig. 1(B)). The GAGG block was optically coupled to a Si-PM array (Hamamatsu MPPC S11064-050P) (Fig. 1(C)). The Si-PM array has 4×4 channels whose size is 3×3 mm^2. The number of pixels per Si-PM of the array is 3600 and the pixels size is 50×50 um^2.

2.2. Dual-head coincidence imaging system using Si-PM-based GAGG block detectors

2.2.1. Dual-head coincidence imaging system

A dual-head coincidence imaging system using the two GAGG block detectors is shown in Fig. 2(A). Two Si-PM-based GAGG block detectors were positioned at the top of the flexible arm. One lineally moves to change the distance between the block detectors. The flexible arm was installed on an X–Y–Z table that can precisely move the dual-head coincidence imaging system in any direction.

Fig. 2(B) shows the system's detector part. The GAGG block detectors are housed in 5-mm thick tungsten plastic containers (density: 12) to reduce the gamma ray from outside the field-of-view (FOV). Tungsten plastic was employed due to its low manufacturing cost compared with tungsten. The Si-PM signals were fed to the electronics with 1.2 m long fine coaxial cables.

2.2.2. Electronics circuit and data acquisition system

The Si-PM array signals were individually amplified by voltage feedback high-speed operational amplifiers and summed for rows and columns using summing amplifiers. Such signals were weighted summed with position dependent linear gains for each row and column signals to produce weighted sum signals. These weight summing calculations were performed using operational amplifiers and produced two weight summed signals for two opposite X directions (X^+ and X^-) and Y directions (Y^+, and Y^-). These weight summed signals were analog-to-digital (A–D) converted using four free running A–D converters (100 MHz). Signals exceeding the threshold were digitally integrated for 470 ns. The 2-dimensional position histogram was derived by calculating the center of gravity for the X and Y positions ($X^+/(X^+ + X^-)$ and $Y^+/(Y^+ + Y^-)$), and the energy was calculated by $(X^+ + X^-)$ for each pixel of the 2-dimensional position histogram. These calculations were performed digitally by field programmable gate array (FPGA). This electronics circuit is the same as that used for the Si-PM-based PET system [8]. The same temperature dependent gain control system as employed for the Si-PM-based small animal PET system was also used [17].

2.2.3. Image formation

All coincidence lines of responses between two GAGG block detectors were acquired in a list mode. Planner images were derived using a focal plane method to form a 39×33 matrix data. The pixel size was 0.3×0.3 mm^2. Detector pixel number differences within ± 2 were added to the pixel, similar concept to the single slice rebinning used for PET image reconstruction. The normalized data were measured using a plane phantom

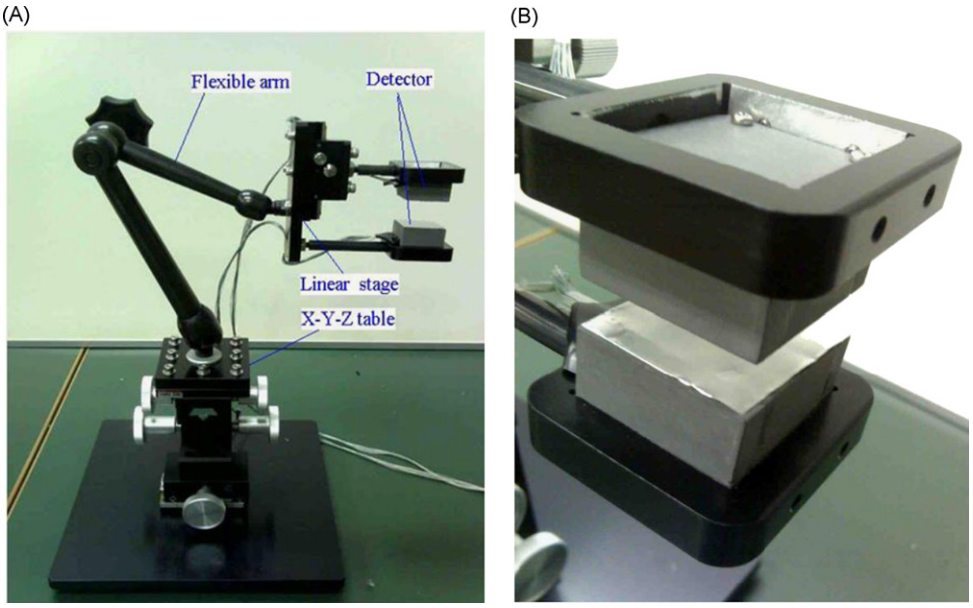

Fig. 2. Si-PM-based dual-head coincidence imaging system (A) and detector part of system (B).

containing F-18 (solution thickness: 5 mm), and the acquired data were divided by the normalized data to correct the detector pair sensitivity differences. With this normalization procedure, the sensitivity difference was almost completely eliminated.

2.3. Performance evaluation

2.3.1. Light output and energy resolution comparisons of GAGG and LYSO

To measure the quality of the GAGG used for the block detectors, the light output and energy resolution performance of the GAGG scintillator was compared with a LYSO. The GAGG scintillator ($5 \times 5 \times 5$ mm^3) (Furukawa Machine and Metal Co., Tokyo) was wrapped with Teflon tape and optically coupled at the center of a Si-PM array (Hamamatsu MPPC S11064-050P) with a 2-mm thick light guide. Silicon rubber (Shin-etsu Silicone, KE-420) was used for the optical coupling. The signal from the Si-PM array was fed to the same electronics and data acquisition system as used for the dual-head coincidence imaging system. Next, the GAGG was removed from the Si-PM array, a LYSO scintillator ($5 \times 5 \times 5$ mm^3) wrapped in Teflon tape was optically coupled to the PMT, and data were acquired. The same silicon rubber was used for the optical coupling. The LYSO used for the comparison was $Lu_{1.8}Y_{0.2}SiO_5$:Ce (Saint-Gobain Crystals, Ohio, USA). Measurements were made for Cs-137 (662 keV) gamma sources. The same supplied voltage (-70.1 V) was used for both measurements. The photopeak channel number and energy resolution were measured.

2.3.2. Positioning performance

The gamma ray from Cs-137 was irradiated uniformly to the GAGG block detector to acquire the 2-dimensional position histogram. The energy threshold level was set at approximately ~20% of the photopeak. Profiles along the GAGG crystals 10th in the horizontal and 9th in vertical directions were used to evaluate the peak-to-valley ratio (P/V) of the GAGG pixel separations.

2.3.3. Energy response

The energy resolution was measured by setting the position boundaries on the 2-dimensional position histogram measured for the Cs-137 point source. Then we calculated the energy spectra for the 20×17 GAGG pixels. The energy resolutions for the central GAGG crystals in the horizontal and vertical directions were used to evaluate the average energy resolution.

2.3.4. Spatial resolution

The spatial resolution of the dual-head coincidence imaging system was measured using a Na-22 point source whose diameter was 0.25 mm. The Na-22 point source was positioned at the center of the FOV. The distance between the two GAGG block detectors was 30 mm. Data were acquired for 10 min, and the spatial resolution was evaluated from the profile of the point source image.

2.3.5. Sensitivity

The sensitivity profile of the dual-head coincidence imaging system was measured using a Na-22 point source moving between the GAGG block detectors, and the count rate was measured. To measure the sensitivity as a function of the distance between the block detectors, the Na-22 point source was positioned at the center of the GAGG block detectors, and the count rate was measured by changing the distance. Sensitivity was derived by dividing the count rate by the radioactivity of the Na-22 point source.

2.3.6. Timing characteristics

Using the dual-head coincidence imaging system, we measured the timing characteristics. After positioning a Na-22 point source between the block detectors with 30 mm detector separation, the coincidence events were acquired with the differences of the two arrival times. The timing spectrum was derived by sorting the differences of the two arrival times.

2.3.7. Temperature characteristics

The temperature characteristics of the dual-head coincidence imaging system were measured with and without the temperature dependent gain control system by the positions of the Na-22 point source between the block detectors with 30 mm detector separation. After the lower energy threshold was set to 350 keV at 20 °C, the temperature was changed from 20 to 24 °C, and the coincidence count rates were monitored. During the measurements, the temperature was measured inside the tungsten plastic-based container

of one of the block detectors. With correction, the temperature dependent gain correction factors were applied every second. Without correction, a single correction value at 20 °C was applied.

2.3.8. Phantom, small animal and plant studies

To demonstrate the imaging performance of the dual-head coincidence imaging system, we imaged a phantom, a rat, and a plant. For imaging the phantom, the central part of a bar-pattern phantom was imaged (Fig. 3(A)) at widths of 2.5, 2, 1.5, and 1 mm. Approximately 7.4 MBq (200 μCi) of F-18-solution was contained in the grooved bar part of the phantom, which was imaged between the dual-head coincidence imaging system with a distance between the block detectors of ~15 mm. The acquisition time was 30 min.

For rat imaging, images of the left paw's finger were acquired. Approximately 74 MBq (2 mCi) of F-18-NaF (F minus) was intravenously administered to a normal rat from the tail vein under anesthesia. The study was performed under the guidelines of the Laboratory Investigation Committee of the Osaka University Graduate School of Medicine. The rat was imaged by the dual-head coincidence imaging system at ~10 mm between the block detectors. The acquisition time was 30 min.

For plant imaging, a radish sprout was dipped into ~18 MBq (500 uCi) of F-18-NaF (F minus) solution for approximately 1 h and pasted on a 2-mm thick plastic plate. The plant leaf was positioned between the dual-head imaging system at 10 mm between the block detectors and images were acquired for 30 min (Fig. 3(C)).

3. Results

3.1. Performance evaluation

3.1.1. Light output comparison

The plots in Fig. 4(A) and (B) show the energy spectra measured with the GAGG and LYSO crystals measured for the Cs-137 gamma ray. GAGG had the photopeak in a 1.25 times higher channel number. The energy resolutions of GAGG and LYSO for the Cs-137 gamma ray were 7.7% and 9.0% FWHM. The photo-fraction (photo-peak counts/ Compton scatter counts) of GAGG is smaller than that of LYSO since the density and atomic number of GAGG are smaller than those of LYSO.

3.1.2. Positioning performance

The 2-dimensional position histograms of the GAGG block detector for the Cs-137 gamma ray are shown in Fig. 5. The 2-dimensional

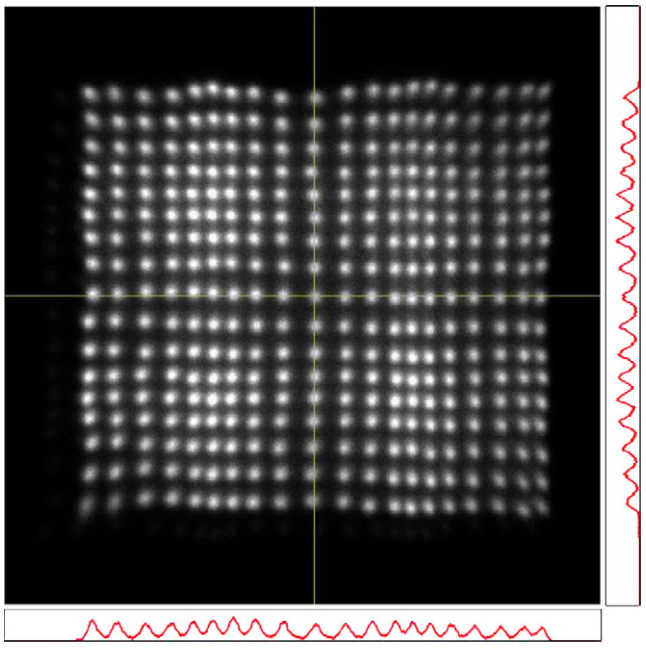

Fig. 5. 2-dimensional position histogram for Cs-137 (662 keV) gamma ray.

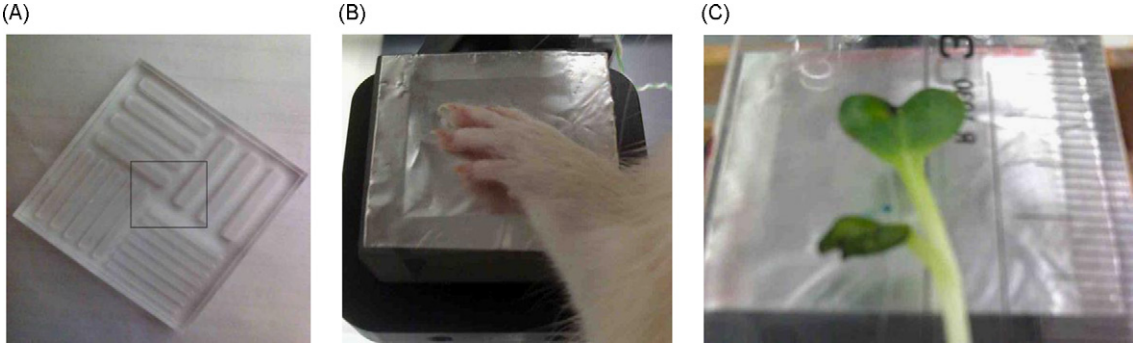

Fig. 3. Photograph of the objects used with dual-head imaging bar-pattern phantom (A), rat fingers (B), and radish sprout (C). Square part in (A) indicated area imaged by imaging system.

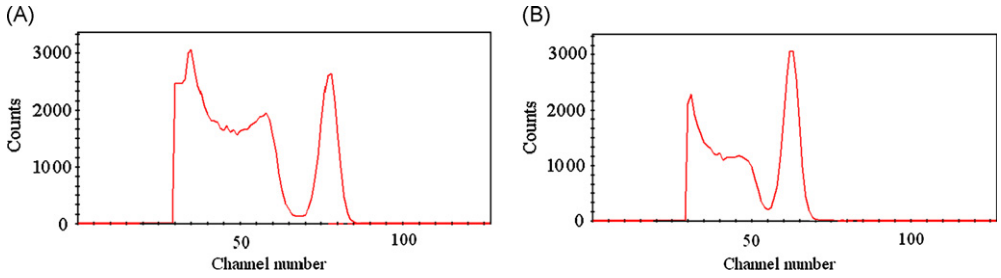

Fig. 4. Energy spectra of GAGG (A) and LYSO (B) for Cs-137 (662 keV) gamma ray.

position histogram for the 662 keV gamma ray was clearly resolved with an average P/V ratio of 3.8.

3.1.3. Energy response for GAGG block detector

In Fig. 6, a typical energy spectrum of a GAGG pixel for Cs-137 (662 keV) gamma ray is shown. The average energy resolution was 14.4% FWHM.

3.1.4. Spatial resolution

The image and profile of the Na-22 point source measured by the dual-head coincidence imaging system are shown in Fig. 7(A) and (B). The spatial resolution was 0.7 mm FWHM.

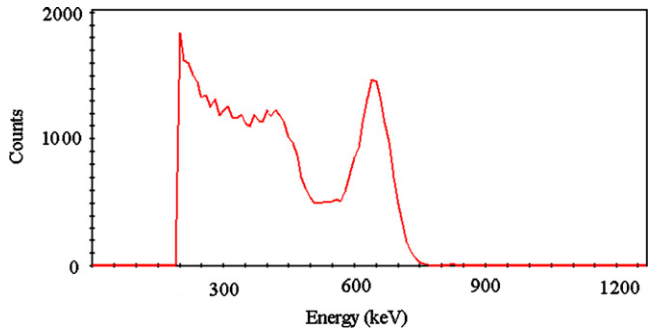

Fig. 6. Energy spectrum of one GAGG pixel for Cs-137 (662-keV) gamma ray.

3.1.5. Sensitivity

In Fig. 8(A), the sensitivity profile of the dual-head coincidence imaging system is shown along the horizontal direction when the block detector separation was 30 mm. The sensitivity was 0.012% at the center of the coincidence imaging system. The sensitivity as a function of the distance between the two block detectors is shown in Fig. 8(B). It dramatically increased when the distance decreased between the block detectors.

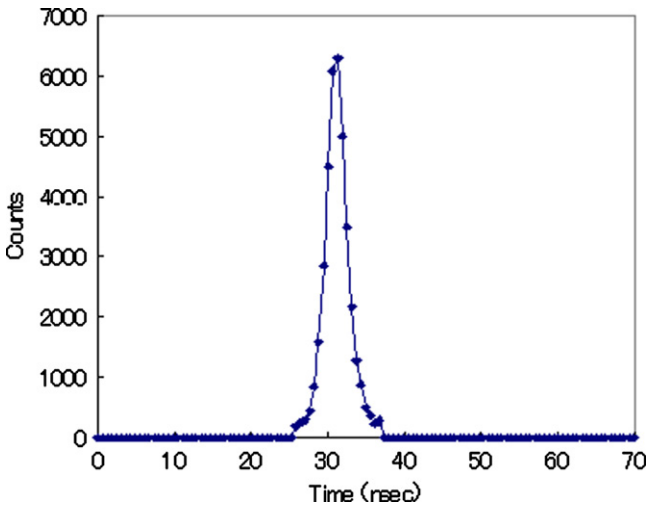

Fig. 9. Timing spectrum of Si-PM-based GAGG coincidence imaging system.

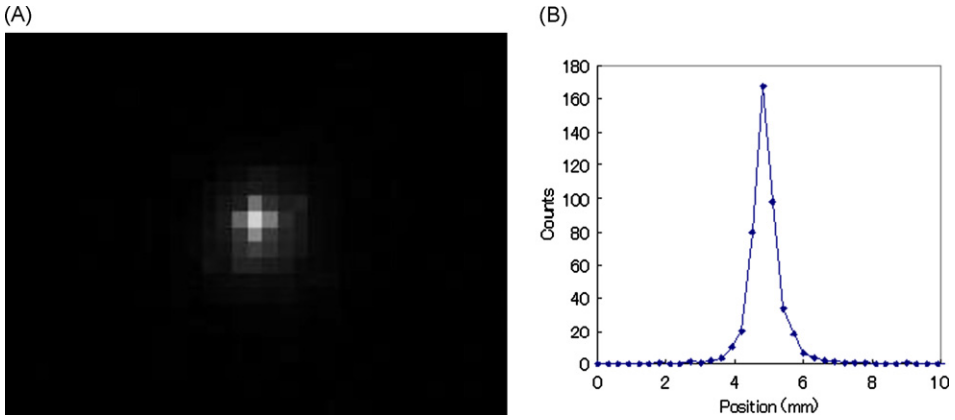

Fig. 7. Image of point source (A) and profile of image (B) of Na-22 point source.

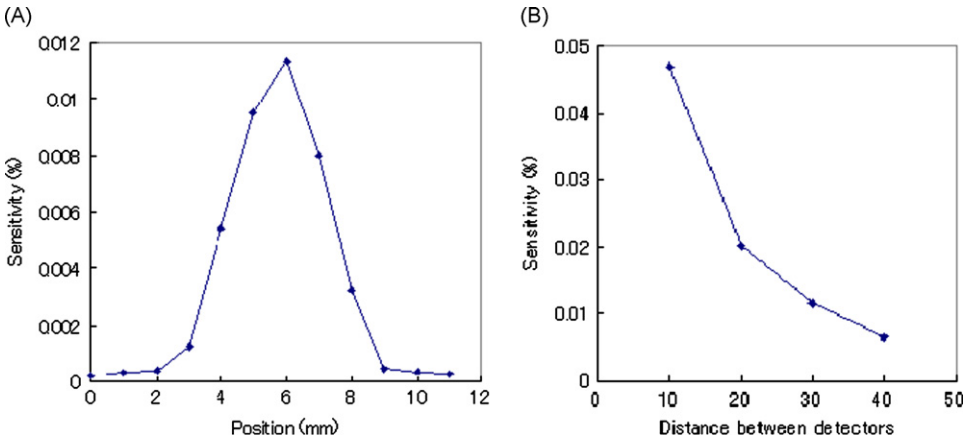

Fig. 8. Sensitivity profile of dual-head coincidence imaging system along horizontal direction (A) and sensitivity as a function of distance between two block detectors (B).

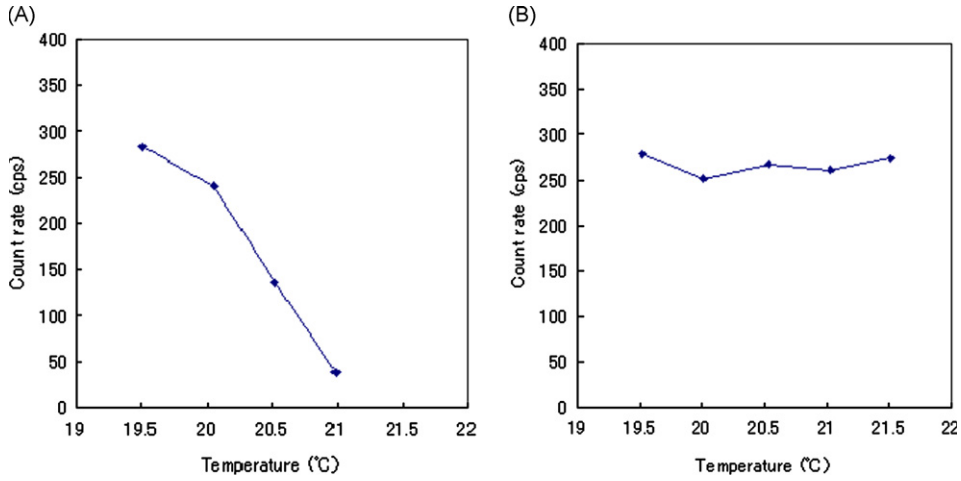

Fig. 10. Temperature characteristics of dual-head coincidence imaging system without (A) and with (B) temperature dependent gain correction.

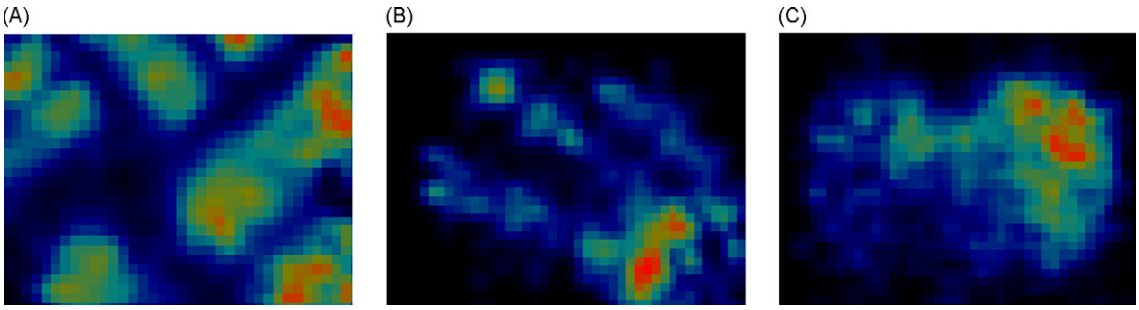

Fig. 11. Image of bar-pattern phantom (A), rat fingers (B), and radish sprout (C).

3.1.6. Timing characteristic

The timing spectrum of the dual-head coincidence imaging system is shown in Fig. 9. The timing resolution was 3 ns FWHM.

3.1.7. Temperature characteristic

Fig. 10 shows the temperature characteristics of the dual-head coincidence imaging system. Its coincidence count rate dropped to 10% of that of 19.5 at 21 °C without correction. With correction, the count rate was within $\pm 5\%$ from 19.5 to 21.5 °C.

3.1.8. Phantom, small animal, and plant studies

Bar-pattern phantom, rat fingers, and radish sprout images are shown in Fig. 11(A), (B), and (C), respectively. In the bar-pattern phantom, the bar-pattern structure of the central part of the phantom is observed. In the rat claw image of F-minus, the structure of the bone of the three claws is seen. In the radish sprout image of F-minus, accumulation of F-minus in the leaf was observed.

4. Discussion

We successfully developed a Si-PM-based GAGG coincidence imaging system. GAGG has advantages over LYSO or LGSO in Si-PM-based coincidence imaging systems. First, higher signals can be obtained when it is combined with Si-PM arrays (Fig. 4). The higher signals improve the position performance and the energy resolution of the block detectors. Compared with our previously developed LGSO block detectors [10], smaller size pixels could be resolved as well as energy resolution was slightly better [10] for the presented GAGG block detector even though the pixel size was smaller. This characteristic is suitable for ultrahigh-resolution imaging detectors. Second, GAGG does not contain natural radioactivity since it does not use Lu. The scintillators containing Lu, such as LSO, LYSO, and LGSO, have problems from beta-gamma true coincidence [18] when the lower energy threshold is low. When two block detectors are positioned with a small distance in the dual-head imaging system, the probability of gamma ray detection from the Lu of the opposite detector increases. The increase of random coincidence also becomes a problem during measurement at low activity.

Although GAGG has advantages for Si-PM-based block detectors, there are some disadvantages. First, since the density and the effective atomic number of GAGG are smaller than LYSO or LGSO, the sensitivity of the coincidence imaging system becomes lower. Comparing the energy spectra of GAGG and LYSO (Fig. 4), the photo-fraction of GAGG is smaller than LYSO. Second, the scintillation decay time of GAGG is slower than LYSO or LGSO, limiting the count rate performance.

The energy resolution of GAGG in the block (Fig. 6) is worse than that of the $5 \times 5 \times 5$ mm^3 GAGG (Fig. 4(A)), probably because of the light attenuation in the small size GAGG in the block ($0.5 \times 0.5 \times 5$ mm^3). However, since the reflector material used for our GAGG block was efficient, the degradation of the energy performance was relatively small. The reflector selection will be important in such block detectors with very thin scintillators to obtain good energy performance.

Our developed dual-head coincidence system was useful for imaging small animals and plants. Since the imaging system can only obtain planner images, such thin subjects as leaves are suitable to image. Although a BGO-based dual-head coincidence imaging system was developed and used for plant research [19–22], the system's spatial resolution was limited to be more than 2 mm since the size of the BGO scintillators used was 2 mm.

Compared with these planner coincidence image system, the developed Si-PM-based GAGG coincidence imaging system has much higher resolution (0.7 mm) with 0.5 mm GAGG scintillators. The high resolution of the imaging system will be useful to observe the smaller parts of subjects and has potential to be used for new applications in molecular imaging.

5. Conclusions

We developed an ultrahigh-resolution Si-PM-based dual-head coincidence imaging system with less than 1 mm resolution by the use of GAGG scintillators. Our developed dual-head coincidence imaging system is promising for small animal and plant imaging research.

Acknowledgments

We thank Drs. Kawachi and Fujimaki of the Japan Atomic Energy Agency for their advice on plant imaging. We also thank Mr. Ohta for designing and manufacturing some of the mechanical parts of the system. This work was partly supported by the Ministry of Education, Science, Sports and Culture, Japan and the Japan Science and Technology Association, Japan.

References

[1] E. Tanaka, T. Hiramoto, N. Nohara, Journal of Nuclear Medicine 11 (1970) 542.
[2] A.N. Otte, J. Barral, B. Dolgoshein, J. Hose, S. Klemin, E. Lorenz, et al., Nuclear Instruments and Methods in Physics Research Section A 545 (2005) 705.
[3] P. Finocchiaro, A. Pappalardo, L. Cosentino, M. Belluso, S. Billotta, G. Bonanno, S.D. Mauro, IEEE Transactions on Nuclear Science 56 (2009) 1033.
[4] D.R. Schaart, H.T. van Dam, S. Seifert, R. Vinke, P. Dendooven, H. Löhner, F.J. Beekman, Physics in Medicine and Biology 54 (2009) 3501.
[5] A. Kolb, E. Lorenz, M.S. Judenhofer, D. Renker, K. Lankes, B.J. Pichler, Physics in Medicine and Biology 55 (2010) 1815.
[6] G. Llosá, N. Belcari, M.G. Bisogni, G. Collazuol, S. Marcatili, M. Boscardin, M. Melchiorri, et al., Nuclear Instruments and Methods in Physics Research Section A 610 (2009) 196.
[7] G. Llosá, N. Belcari, M.G. Bisogni, G. Collazuol, S. Marcatili, P. Barrillon, C. de la Taille, S. Bondil-Blin, N. Dinu, M. Melchiorri, et al., IEEE Transactions on Nuclear Science 56 (2009) 2586.
[8] S. Yamamoto, M. Imaizumi, T. Watabe, H. Watabe, Y. Kanai, E. Shimosegawa, J. Hatazawa, Physics in Medicine and Biology 55 (2010) 5817.
[9] S.I. Kwon, J.S. Lee, H.S. Yoon, M. Ito, G.B. Ko, J.Y. Choi, S.H. Lee, I. Chan Song, J.M. Jeong, D.S. Lee, S.J. Hong, Journal of Nuclear Medicine 52 (2011) 572.
[10] S. Yamamoto, H. Watabe, J. Hatazawa, Physics in Medicine and Biology 56 (2011) N227.
[11] S. Yamamoto, H. Watabe, Y. Kanai, M. Imaizumi, T. Watabe, E. Shimosegawa, J. Hatazawa, Physics in Medicine and Biology 56 (2011) 7555.
[12] K. Kamada, T. Yanagida, T. Endo, K. Tsutsumi, Y. Usuki, M. Nikl, Y. Fujimoto, A. Fukabori, Y. Yoshikawa, Journal of Crystal Growth 352 (2011) 88.
[13] H. Uchida, T. Okamoto, T. Ohmura, K. Shimizu, N. Satoh, T. Koike, et al., Nuclear Instruments and Methods in Physics Research Section A 516 (2004) 564.
[14] Hui Zhang, Qinan Bao, T.Vu Nam, W. Silverman, Richard Taschereau, N. Berry-Pusey, Ali Douraghy, R. Rannou, B. Stout, F. Arion, Molecular Imaging and Biology 13 (2011) 949.
[15] J. Seidel, Wenze Xi, J.W. Kakareka, T.J. Pohida, M.V. Green, P.L. Choyke, IEEE Nuclear Science Symposium Conference Record (NSS/MIC) (2010) 2206.
[16] T. Yanagida, A. Yoshikawa, Y. Yokota, K. Kamada, Y. Usuki, S. Yamamoto, et al., IEEE Transactions on Nuclear Science 56 (2009) 10.
[17] S. Yamamoto, J. Satomi, T. Watabe, H. Watabe, Y. Kanai, M. Imaizumi, E. Shimosegawa, J. Hatazawa, Physics in Medicine and Biology 56 (2011) 2873.
[18] S. Yamamoto, H. Horii, M. Hurutani, K. Matsumoto, M. Senda, Annals of Nuclear Medicine (2005).
[19] H. Uchida, T. Okamoto, T. Ohmura, K. Shimizu, N. Satoh, T. Koike, et al., Nuclear Instruments and Methods in Physics Research Section A 516 (2003) 564.
[20] N. Kawachi, K. Kikuchi, N. Suzui, S. Ishii, S. Fujimaki, N.S. Ishioka, H. Watabe, IEEE Transactions on Nuclear Science 58 (2011) 395.
[21] S. Ishii, N. Suzui, S. Ito, N.S. Ishioka, N. Kawachi, N. Ohtake, T. Ohyama, S. Fujimaki, Soil Science and Plant Nutrition 55 (2009) 660.
[22] R. Suwa, S. Fujimaki, N. Suzui, N. Kawachi, S. Ishii, K. Sakamoto, N.T. Nguyen, H. Saneoka, P.K. Mohapatra, R.E. Moghaieb, Plant Science 175 (2008) 210.